A strong enhancement of corrosion and wear resistance of polyurethane-based coating by chemically grafting of organosolv lignin

Materials Today Chemistry 35 (2024) 101833

Contents lists available at ScienceDirect

Materials Today Chemistry

journal homepage: www.journals.elsevier.com/materials-today-chemistry/

A strong enhancement of corrosion and wear resistance of polyurethane-based coating by chemically grafting of organosolv lignin

Di Wang [a], Jun Zhao [a], Per Claesson [b], Paul Christakopoulos [c], Ulrika Rova [c], Leonidas Matsakas [c], Erik Ytreberg [d], Lena Granhag [d], Fan Zhang [e,**], Jinshan Pan [b,***], Yijun Shi [a,*]

[a] Division of Machine Elements, Department of Engineering Sciences and Mathematics, Luleå University of Technology, Luleå, SE-971 87, Sweden
[b] Division of Surface and Corrosion Science, Department of Chemistry, KTH Royal Institute of Technology, Stockholm, SE-100 44, Sweden
[c] Division of Chemical Engineering, Department of Civil, Environmental and Natural Resources Engineering, Luleå University of Technology, Luleå, SE-971 87, Sweden
[d] Department of Mechanics and Maritime Sciences, Chalmers University of Technology, SE 412 96, Gothenburg, Sweden
[e] Department of Engineering and Design, School of Engineering and Information, University of Sussex, Brighton, BN1 9RH, United Kingdom

ARTICLE INFO

Keywords:
Organosolv lignin
Polyurethane
Coating
Anti-corrosion
Wear resistance

ABSTRACT

Corrosion and wear pose significant challenges to equipment operating in harsh environments. Thus, protective coatings are needed. Anti-corrosion and anti-wear coatings are traditionally fossil-based and often contain environmentally harmful additives. Achieving anti-corrosion and anti-wear coatings based on environmentally benign and sustainable materials is important and a significant challenge. This work focused on the development of organosolv lignin-based polyurethane (OS_lignin-PU) coatings. The coatings were synthesised and evaluated for corrosion protection using electrochemical impedance spectroscopy (EIS) and for wear properties using nanoindentation and nano scratch measurements. EIS revealed that the optimal lignin content for corrosion protection purposes in the OS_lignin-PU coatings was 15 wt%. Moreover, addition of 15 wt% lignin to the OS_lignin-PU coatings also enhanced their wear resistance, as evidenced by reduced thickness loss during tribometer tests. The nano scratch measurements revealed that OS_lignin-PU coatings containing 15 wt% lignin exhibited the lowest scratch depth and friction coefficient. It is found that the developed lignin-containing coating exhibits remarkable corrosion and wear resistance, making it a promising sustainable material in various applications for pursuing sustainable development.

1. Introduction

Nowadays, marine human activities, such as ships, pipelines, offshore platforms, and aquaculture equipment, have increased rapidly with our population growth [1]. The harsh environment in ocean from the aggressive nature of seawater, various organisms, hydrostatic pressure, and water movement jointly pose a challenge to the application of marine equipment for long periods of time [2–4]. In order to protect the equipment, coatings, especially anti-corrosion coatings, are widely needed [5–7]. Corrosion is the most common cause of significant economic loss in industry and poses serious safety risks [8]. Using anti-corrosion coatings is an effective method to protect products from corrosion and thus prolong their service life. Traditional coatings use additives, such as chromate, that harm the environment and marine organisms [9,10]. Therefore, using environmentally friendly anti-corrosion coatings to replace toxic and harmful coatings is becoming the consensus of the industry.

Anticorrosive coatings are also degraded by environmental impact, and wear by waves, wind, floats, sand, etc., is a serious problem [11]. Coatings in the splash zone are more susceptible to the synergistic negative effects of wear and corrosion that accelerate degradation [12]. In addition, many coatings are damaged before components are put into operation due to wear [11]. Galvanic corrosion is often initiated by cracks or pinholes in the coating that form due to wear, which ultimately leads to coating failure [13]. Therefore, increasing the wear resistance of coatings is essential for improving their durability.

Lignin is an abundant bio-based material that is a by-product of the paper industry, but it has found limited applications for decades [14].

* Corresponding author.
** Corresponding author.
*** Corresponding author.
E-mail addresses: zhangfan@sussex.ac.uk (F. Zhang), jinshanp@kth.se (J. Pan), yijun.shi@ltu.se (Y. Shi).

https://doi.org/10.1016/j.mtchem.2023.101833
Received 7 July 2023; Received in revised form 12 November 2023; Accepted 26 November 2023
Available online 8 December 2023

However, lignin has been explored in high-value products by using it as an ingredient for polymer synthesis [15], adsorbents [16], precursors for carbon materials [17,18] and UV protectors [19]. One of lignin's promising applications is as a functional additive in coatings. Recently, it has been utilised in anti-corrosion and anti-wear coatings due to its antioxidant activity, stability and biodegradability [20–23]. However, limited compatibility with specific polymer matrices and challenges in achieving uniform coatings have limited the widespread application of lignin coatings. Organosolv lignin has the improved solubility in organic solvents like acetone and n-dimethylformamide (DMF), providing reaction condition between lignin and isocyanate. Polyurethane has been widely used in adhesives and coatings. As a mature commercial polymer material, polyurethane has the characteristics of high toughness, good corrosion resistance and wear resistance, and this material has been widely used in anti-corrosion coatings [24–26]. However, most polyurethane materials are fossil-based and not recycled nowadays. It is thus, in these aspects, less environmentally friendly compared to biodegradable and renewable alternatives [27]. Therefore, synthesising anti-corrosion polyurethane coatings with high lignin content by a simple process could reduce the environmental impact of PU and improve the corrosion and wear resistance of coatings.

In this work, lignin-modified polyurethane (lignin-PU) is synthesised from polycarbonate polyols (PPC), 4,4′-dicyclohexylmethane diisocyanate (HMDI) and lignin. The corrosion resistance of the resulting coatings is evaluated by means of electrochemical impedance spectroscopy (EIS). The expected corrosion resistance of lignin-PU is higher than that of pure polyurethane. The coating's wear properties are evaluated by nanoindentation test, nano scratch test and friction test. Samples with different lignin content were prepared to identify the optimal lignin content for corrosion and wear protection.

2. Experiment

2.1. Materials

Polycarbonate polyols (PPC) ($M_n \approx 2000$ g/mol) was purchased from Huizhou Dayawan Dazhi Fine Chemical Co., Ltd., P.R. China. 4,4′-dicyclohexylmethane diisocyanate (HMDI, 99%) (Mn ≈ 262.35 g/mol) and 1,2-ethanediol were purchased from Wan Hua Chemical, P.R. China. Lignin was extracted according to the method in previous work [28]. The method is described in supporting information. Dibutyltin dilaurate (DBTDL, 95%) and N, N-dimethylformamide (DMF, 99.5%) were purchased from Sigma-Aldrich. Carbon steel DC01 was used as the substrates, and its chemical composition is shown in Table S1.

2.2. Polymer synthesize and preparation

2.2.1. Synthesis of lignin chemically grafted polyurethane

A certain amount of lignin was first dissolved in DMF and reacted with HMDI at 90 °C under stirring. During the reaction, DBTDL was added as the catalyst. After 3 h of reaction, dehydrated PPC was added into the solution and kept in the reaction condition for another 6 h. The mass fraction of lignin in the final dry coating was controlled at 0 wt%, 5 wt%, 10 wt%, 15 wt% and 19 wt%, and the corresponding solutions were noted as PU, C5, C10, C15 and C19. Since the PU sample, which only had HMDI reacted with PPC, cannot be cured due to low hard segment content in polymers, 1,2-ethanediol was used to promote the curing of the PU sample. The specific chemical composition of each material is shown in Table S2, and the synthesis route of Lignin-PU is shown in Fig. 1.

2.2.2. Preparation of lignin physically modified polyurethane

Besides the chemically synthesised lignin-PU, physically mixed lignin and polyurethane coatings were also prepared for comparison. The PU sample introduced in section 2.2.1 was used as matrix coating, and lignin was physically mixed at the same percentage as in the

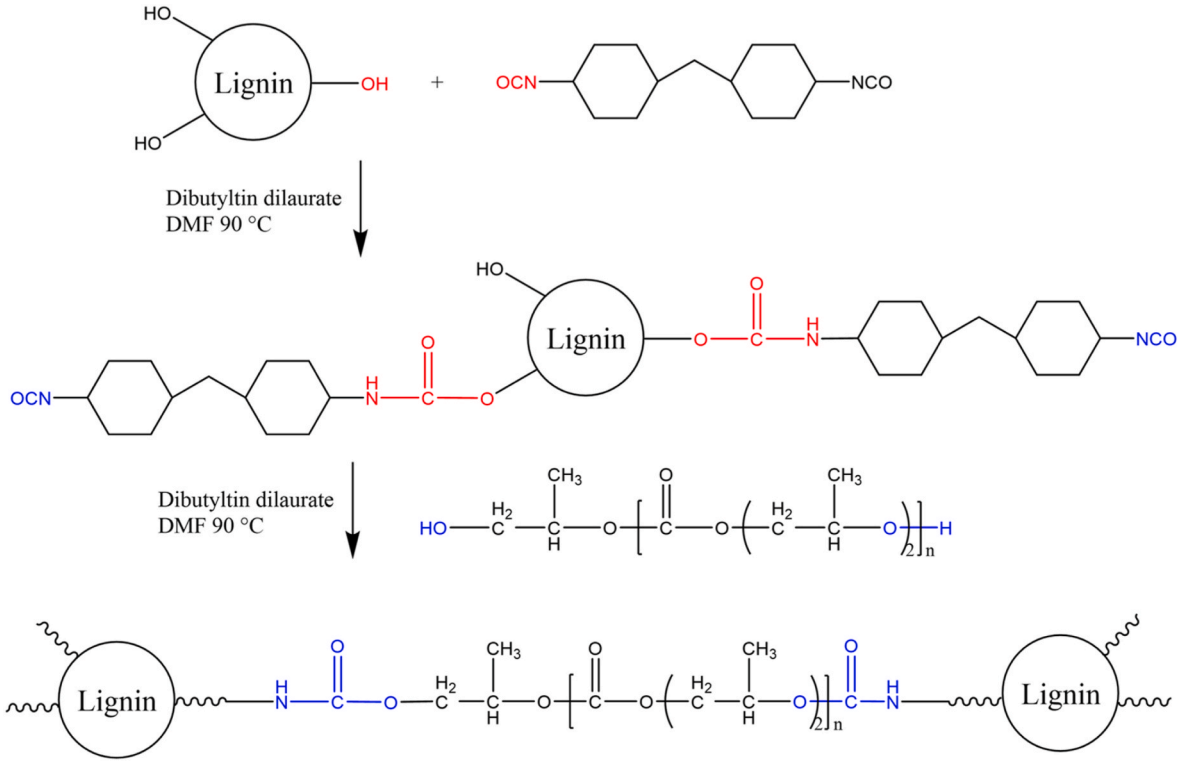

Fig. 1. The synthesis route of Lignin-PU with lignin content from 5 wt% to 19 wt%.

chemically synthesised coatings, which were noted as P5 (for 5 wt% lignin), P10 (for 10 wt% lignin) and P15 (for 15 wt% lignin), respectively. Lignin was dissolved in PU blend under magnetic stirring for 5 h, and the total solid content was controlled at 30 wt%. The mixed blend was applied on steel substrates to form coatings as described below.

2.3. Coating preparation

Carbon steel DC01 was used as the substrate for evaluating corrosion protection performance. Carbon steel sheets with 2 mm thickness were cut to 1.5 × 1.5 cm^2. The surface of the steel electrodes was ground to P1200 using silicon carbide abrasive paper on a MetaServ™ 250 grinder. The rotation speed during grinding was controlled at 200 rpm and water was used to remove the debris during the grinding. The steel electrodes were then ultrasonically cleaned with acetone and ethanol for 10 min in each solvent and dried by compressed air flow. After that, the lignin-PU blend was immediately dropped onto the steel surface and levelled using a MULTICATOR 411 film applicator (ERICHSEN). The dry coating thickness was controlled at 30 μm. The samples were then kept at 20 °C for 24 h to allow the evaporation of the solvent. Finally, the samples were heated to 110 °C and remained 1 h for curing.

2.4. Electrochemical measurement

EIS measurement was conducted using an AutoLab PGSTAT302 N potentiostat (Metrohm, Switzerland). Samples were exposed to 1 mol/L NaCl solution in a three-electrode cell for an accelerated corrosion test. The reference electrode used was saturated Ag/AgCl, and the counter electrode was platinum. The EIS measurements were taken at the open-circuit potential (OCP) with a perturbation amplitude of 10 mV and frequency ranging from 10^4 Hz to 10^{-1} Hz. EIS spectra were collected after 1, 4, 8, 24, 48 and 168 h of immersion.

2.5. Nanoindentation and nano scratch

The nanoindentation and nano scratch experiments were performed using a NanoTest Vantage (Micro Materials). A Berkovich indenter was used for the nanoindentation measurements. The maximum load was 0.15 mN for single load tests, the load time was 30 s, the unload time was 5 s and the dwell time was 5 s. In the multi load tests, the load successively increased from 0.1 mN to 0.2, 0.3, 0.4 and 0.5 mN. The load time was 30 s, the unload time was 5 s, and the dwell time after loading and unloading was 5 s. The nanoindentation experiment was repeated 10 times in parallel for each coating.

The nano scratch measurements were performed using a 90° conical tips indenter with a diameter of 50 μm. Single scratch tests were repeated 10 times in parallel for each coating, with the load of 1 mN, and a load curve is shown in Fig. S1. The scan velocity was set to 5 μm/s and the scan length was 500 μm. Multi scratch data consisted of 10 passes for each coating, including one starting topography pass, eight scan passes and one final topography pass. The load for scan passes were 1 mN, 5 mN and 10 mN, respectively. And the load for topography passes were controlled at 2% of the scan passes. The load details for topography passes and scan passes are shown in Table S3. The loading rate was 0.5 mN/s. The scan velocity was 5 μm/s and the scan length was 500 μm.

2.6. Characterisation

Infrared spectra were measured using a Thermo Scientific Summit Spectrometer. The number of scans was 16, and the resolution was 4 cm^{-1}. The friction tests were conducted using a CETR-UMT 2 tribometer. This setup was reported in our previous work [29]. Wear of the coatings was induced using a reciprocating motion with a frequency of 20 cycles per minute, a stroke length of 3 cm, and an average speed of 2 cm/s at 20 °C. The tests were performed underwater. A 5 N force was applied to a 2 cm^2 contact area with P1200 abrasive paper, generating 25 kPa pressure. The duration of each wear experiment and the test point number is provided in Table 1. Thermogravimetric analysis (TG) was carried out employing a TGA/DSC 3+ thermal analysis system (METTLER TOLEDO) in N_2 atmosphere, with the heating rate of 10 °C/min over the temperature range from 25 to 600 °C. Differential scanning calorimetry (DSC) data was collected by a DSC 3+ thermal analysis system (METTLER TOLEDO). The samples were heated from −50 to 150 °C in N_2 atmosphere with a 10 °C/min heating rate.

3. Results and discussion

In the result section, we first report the characterization of the lignin-PU coatings made by FTIR spectroscopy as well as by TG and DSC. The following sections consider the prepared coatings' corrosion protection properties and wear characteristics.

3.1. FTIR spectra for lignin-PU

The FTIR spectra of both the raw materials and the final lignin-PU coatings are shown in Fig. 2. The characteristic peak of the NCO group appears at 2250 cm^{-1} in HMDI and disappears in the synthesised coating, and the C=O peak related to the carbamate appears at ~1740 cm^{-1}. The peak of OH vibrations at ~3500 cm^{-1} in lignin largely disappears and instead the peak of NH at ~3400 cm^{-1} appears after the reaction, with this disappearance to confirm that the NCO reaction was complete, and carbamate was successfully formed [30,31].

Fig. 3 shows the FTIR spectra of C15 during synthesis. The reaction between lignin and HMDI caused the reduction of the peak from OH vibrations at ~3500 cm^{-1}, as shown in Fig. 3 (a). After adding PPC (Fig. 3 (b)), the peak of NCO at 2250 cm^{-1} decreased, and the peak of NH at ~3400 cm^{-1} increased, suggesting that the reaction proceeded as designed (Fig. 1). The peak of NCO remained in the spectra of C15 blend after reaction. The remaining NCO could react with steel and improve the coating's adhesion. After the curing process, these NCOs were reacted and the spectra in Fig. 2 shows no NCO peak.

It is worth noting that our data also showed evidence of chemical crosslinking within the coating during the curing process. As mentioned earlier, the disappearance of the NCO peak in the FTIR spectra after curing in Fig. 2 indicates that the remaining NCOs in the coating had reacted with other functional groups. One possibility is that the remaining NCOs crosslinked with the remaining OH groups in the lignin, leading to a more compact coating structure. The schematic diagram in Fig. 4 shows that adding lignin could affect the crosslinking degree. Only linear polymers can be produced theoretically when no lignin is involved in the reaction since the degree of functionality for PPC, HMDI, and 1,2-Ethanediol are 2. After adding lignin, which has multiple degree of functionality, a crosslinked network was formed, and the theoretical crosslinking degree concomitantly increased as the lignin content increased [32].

3.2. TG and DSC characterization for lignin-PU

Fig. 5 shows the TG and derivative thermogravimetric (DTG) curves for chemically synthesised lignin-PU coatings. The DTG curves, in combination with TG curves, show that for the lignin-PU coatings, the first stage of thermal degradation occurred at around 250 °C. This is related to the hard segments (1,2-ethanediol and HMDI) [33]. Coating

Table 1
The duration of each wear test and the test point number.

Wear test	Wear test duration (min)	Test point number
–	0	0
#1	3	1
#2	Another 5	2
#3	Another 15	3

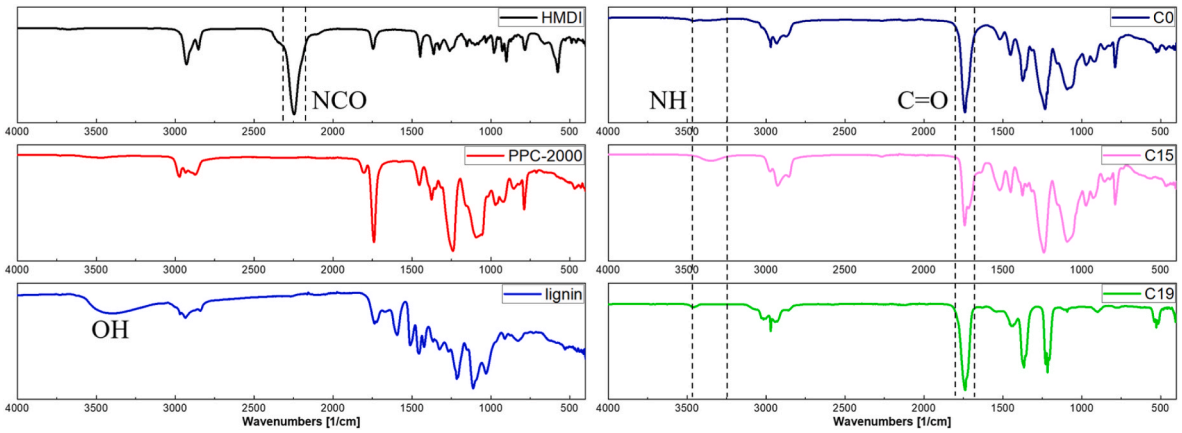

Fig. 2. FTIR ATR spectra of the raw materials and the lignin-PU coatings after curing.

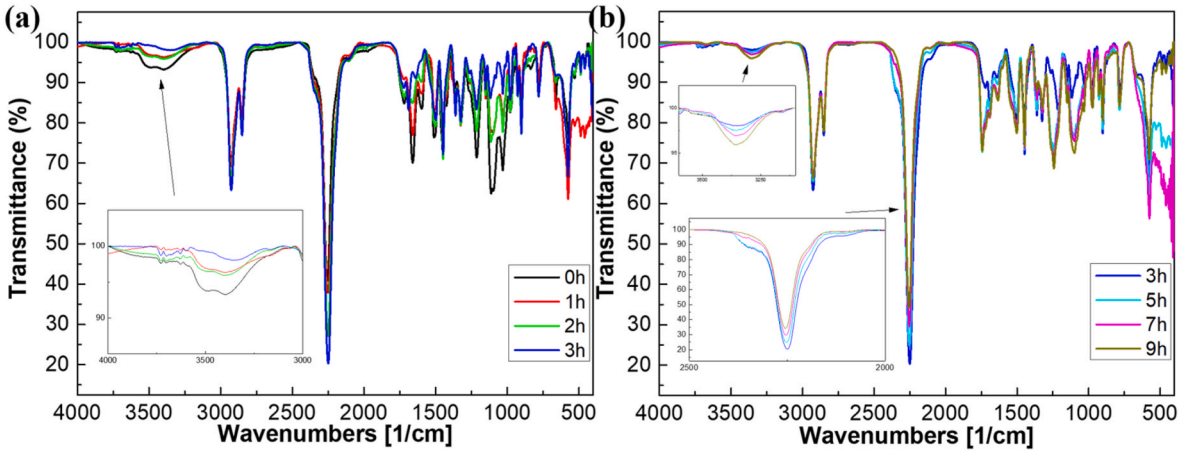

Fig. 3. FTIR ATR spectra of C15 during synthesis. The reaction between (a) lignin and HMDI and (b) PPC, lignin and HMDI.

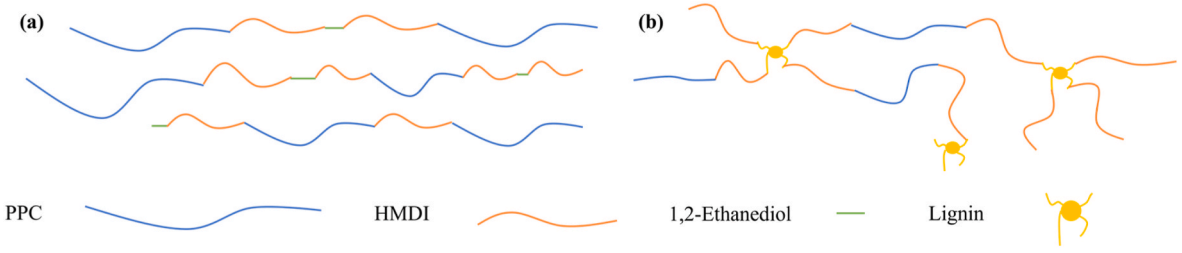

Fig. 4. Schematic diagram for (a) linear and (b) crosslinked polymer.

with 19 wt% lignin was not tested because the coating had poor adhesion to the steel surface and could not form a stable and protective layer. The results of adhesion measurements using the ASTM D3359 standard are shown in Fig. S2. For C5, C10 and C15 coatings the first stage was related to the degradation of HMDI, since the increasing HMDI content led to higher degradation as DTG curve shows. The second stage of degradation for coatings at around 340 °C is probably related to the soft segment content [34]. Adding lignin, which resulted in reduction of PPC, caused the decreased DTG peak. When lignin was added into the coating, the third stage of degradation occurred at around 450 °C probably related to the combustion of the lignin since increasing lignin caused the increasing DTG peak at 450 °C.

Fig. 6 shows the DSC curves for lignin-PU coatings. The glass transition temperature (T_g) for lignin-PU coatings and the range limits used for T_g calculation are shown in Table S4. The T_g increased with increasing lignin content. The T_g of PU coating was −6.2 °C, and when lignin content increased to 15 wt%, the T_g raised to 23.6 °C. The rising T_g shows that the crosslinking degree of lignin-PU was increased with increasing lignin content.

3.3. Corrosion protection of the lignin-PU coating

The Bode plots of impedance modulus and Nyquist plots of the EIS spectra of chemically synthesised lignin-PU coatings with lignin content from 0 to 15 wt% after immersion in 1 M NaCl solution are shown in Fig. 7. The Bode plots of phase angle can be found in Fig. S3. The EIS spectra in Fig. 7 show that all the coatings had resistance values of around 10^8 Ω•cm^2 after 1 h of immersion, indicating similar initial protective ability. During the first 7 days of the exposure, the impedance modulus values at low frequency end (resistance) of the PU, C5, and C10

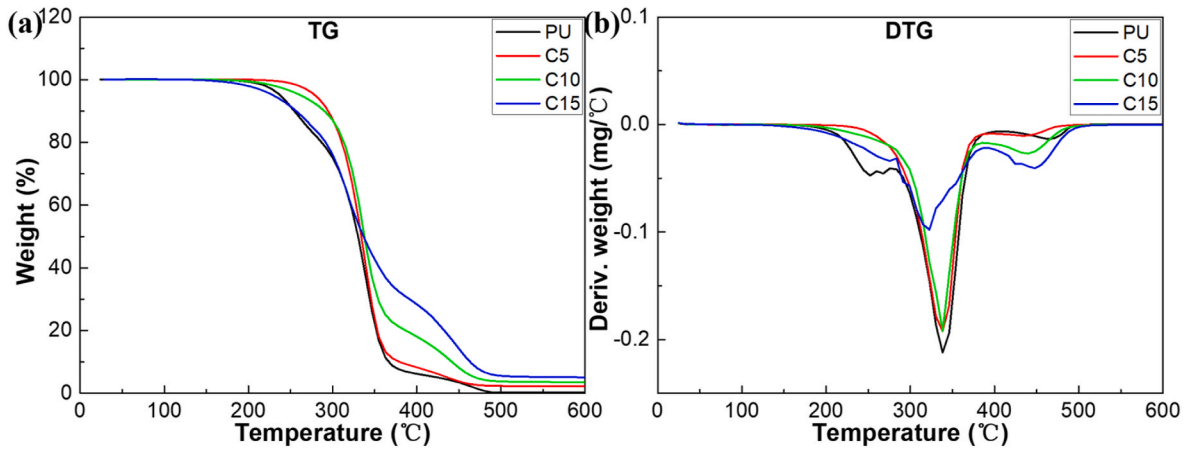

Fig. 5. (a) TG and (b) DTG results for chemically synthesised lignin-PU coatings and the PU coating as comparison.

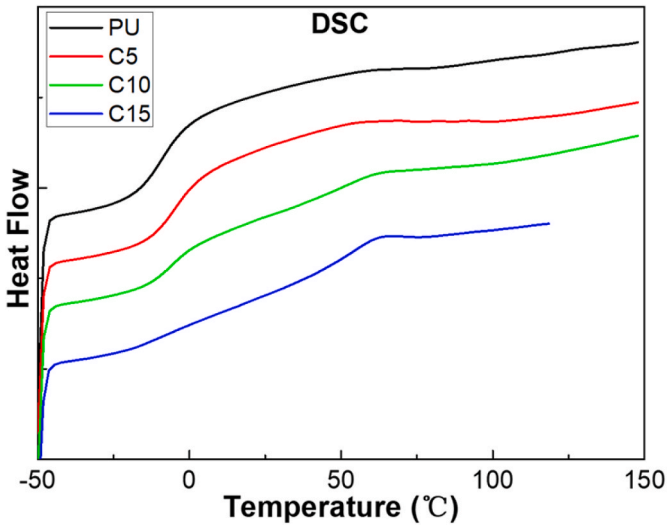

Fig. 6. DSC results for lignin-PU.

coatings decreased by several orders of magnitude compared with the initial value. However, the resistance of C15 coating was still of the order of 10^6 Ω•cm^2, three orders of magnitudes higher than that of bare carbon steel [35]. The results suggest that the lignin-PU coating with 0 wt%, 5 wt% and 10 wt% lignin content quickly deteriorated during exposure, losing the protection ability. In contrast, the lignin-PU coating with 15 wt% lignin maintained its high impedance level, demonstrating a lower coating delamination at the coating/substrate interface after seven days of immersion in the corrosive solution in comparison with other coatings. The impedance modulus at low frequency represents the coatings' capability to hinder the electrochemical current, thus corrosion reaction [36]. After 7 days of immersion, the C15 coating still maintained its corrosion protective ability. The results demonstrated a significant improvement in anti-corrosion properties by adding 15 wt% lignin into lignin-PU coatings.

The EIS spectra of physically mixed lignin-PU coatings with lignin content from 5 to 15 wt% after immersion in 1 M NaCl reveal a much lower impedance level (shown in Figs. S4 and S5) and thus poor protection performance, as compared with chemically synthesised coatings with the same lignin content. A possible explanation is that the free lignin in the coating, with many hydrophilic non-reacted groups, facilitates water absorption and transport to the substrate surface, which promotes electrochemical reactions. Whereas, the chemically modified lignin reaction formed a densely crosslinked network, which hindered the penetration of the solution into the coating and thus enhanced the corrosion resistance of the coating.

The equivalent circuits shown in Fig. 8 (a, b) were applied to fit the EIS data utilizing the Nova software. The simple circuit (a) consists of solution resistance (R_s), polarization resistance (R_p) and constant phase element (CPE) in parallel with it was used for fitting the spectra obtained during initial exposure (with one time constant feature). The polarization resistance R_p was used to evaluate the corrosion resistance of the coating. After extended exposure, the corrosive solution began to permeate the coating and formed a new interface, so circuit (b) was used for spectra fitting [37]. In the circuit (b), R_p changed to R_c (coating resistance), CPE_{dl} represents the capacitor at the new interface, and R_{ct} is the electron transfer resistance [38,39].

The fitting results for lignin-PU coating after 1- and 168-h corrosion tests are shown in Fig. 8(c). After 1 h of exposure, R_p for the pure PU coating was 1.1×10^8 Ω•cm^2. The addition of lignin for 5, 10, and 15 wt % gave an increased R_p value (but of the same orders of magnitude), 2.5×10^8, 2.1×10^8, and 1.5×10^8 Ω•cm^2, respectively. After 168 h (1 week) of exposure, all coatings showed a reduction in R_p. However, the R_p for the C15 coating was significantly higher than for other coatings.

Fig. 8(d) illustrates the fitted Y_0 for lignin-PU coatings at 1 and 168 h of exposure. The following equation expresses the impedance function of a CPE:

$$Z_{CPE} = \frac{1}{(j\omega)^n \bullet Y_0}$$

where Y_0 represents the capacitance of the CPE, and when the dimensionless exponent n equals 1 the CPE is a pure capacitance. The capacitance can be expressed by the parallel-plate model:

$$Y_0 \approx C = \frac{\varepsilon_0 \varepsilon_r A}{d}$$

where ε_0 is vacuum permittivity, ε_r is the dielectric constant of the coating, A is the surface area, and d is the coating thickness. Y_0 had an increasing trend for lignin-PU coatings, while the R_p decreased during corrosion. The value of Y_0 was 1.4×10^{-9} Ω^{-1}cm^{-2}s^n for PU coating at 1 h and it increased to 1.0×10^{-5} Ω^{-1}cm^{-2}s^n at 168 h. For C5 and C10 coatings, Y_0 also raised four to five orders of magnitude after 168 h of exposure. The increased Y_0 fell in the EDL range, suggesting the coating breakdown. Whereas, the Y_0 value for the C15 coating remained at the same magnitude after 168 h of exposure. Since the dielectric constant of water is significantly higher than that of organic coatings, the increase in coating capacitance can be attributed to the penetration of water. Clearly, the dense network formed by the C15 coating limits the water penetration, and this is consistent with the best corrosion protection performance of this coating.

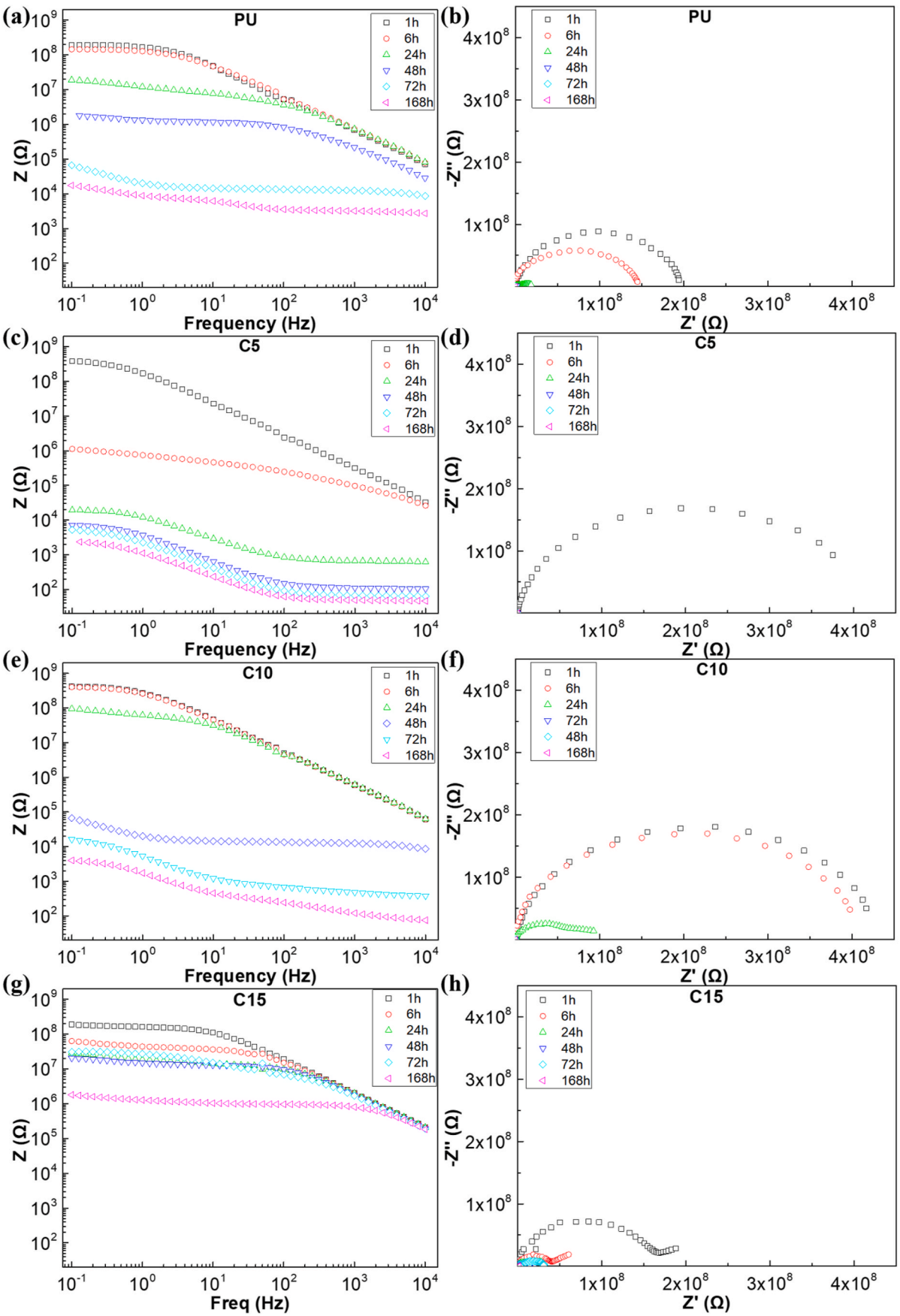

Fig. 7. EIS results show in Bode impedance plots (a,c,e,g) and Nyquist plots (b,d,f,h) for chemically synthesised lignin-PU coating with lignin content increases from 0 to 15 wt%. The exposed area of the coatings was 1 cm^2.

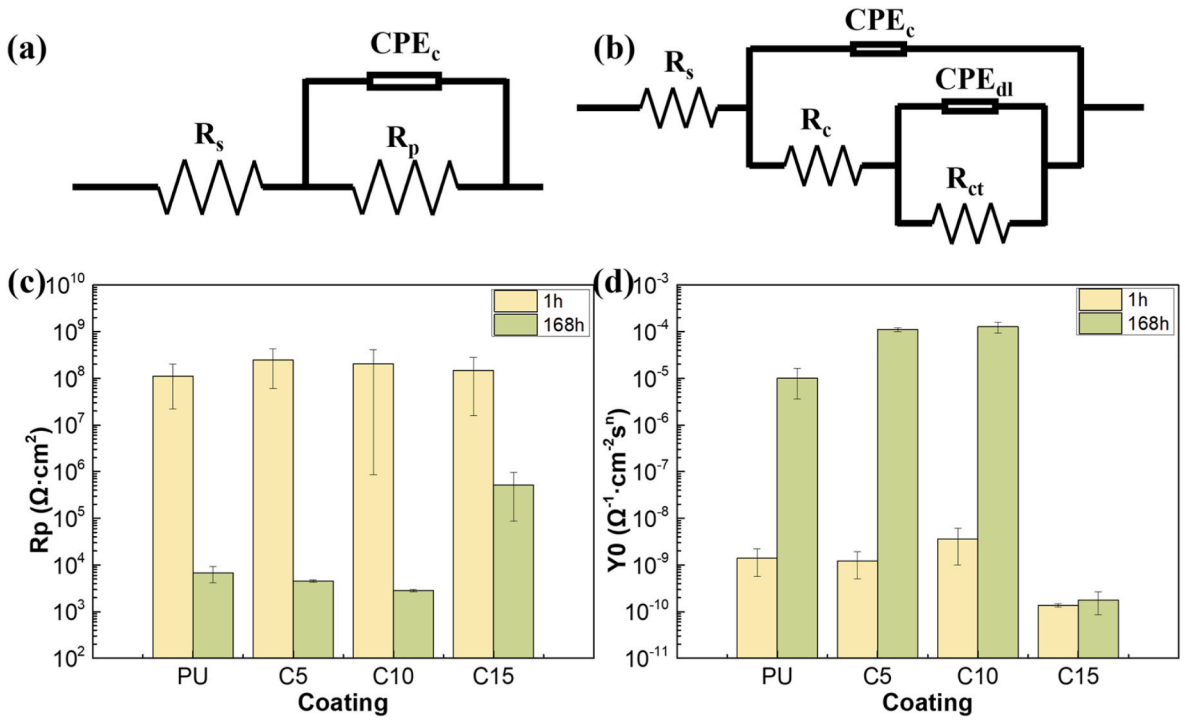

Fig. 8. The equivalent circuit to fit EIS spectra. (a) Simple circuit with one time constant, (b) circuit with two time constant. And fitted R_p (c) and Y_0 (d) after 1- and 168-h corrosion tests for lignin-PU coating.

3.4. Nanoindentation for lignin-PU coating

The load-displacement curves obtained during nanoindentation single load experiments with lignin-PU coatings are reported in Fig. 9. Naturally, the displacement increased with load. Clearly, the PU coating had the highest displacement. Compared to PU coating, C5, C10, and C15 coating shows a decreasing displacement and in particular for C10 and C15, the displacement is very low compared to the other samples. Again, the cross-linked network enhanced by lignin in C10 and C15 significantly changes the material properties. The physically mixed coatings, P5–P15, all had similar deformation, confirming that no cross-linked network was formed. However, even physically mixed lignin with PU, the material became stiffer. There was a sudden recovery before the end of the unloading curve for all coatings, which occurred due to the polymer's viscoelastic behaviour and thermal contraction [40].

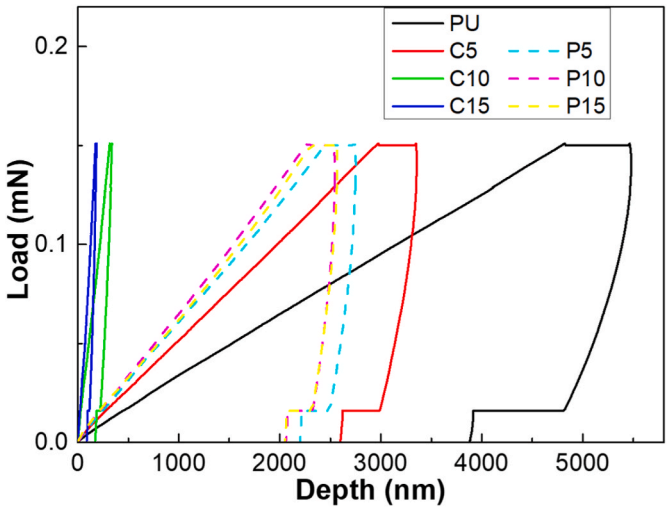

Fig. 9. Load-displacement plots of the lignin-PU coating during single load tests.

The maximum depth and the calculated hardness of lignin-PU coatings are shown in Table 2. The method used to calculate the hardness follows that suggested by Oliver and Pharr [41]. The coating hardness increased from 0.23 MPa for the pure PU coating to 177.12 MPa for C15 coatings. The reason for the escalation of hardness is because of the crosslinked matrix induced by lignin. Moreover, increasing the amount of lignin from 5 wt% to 15 wt% leads to a higher crosslinking degree, thus increasing the coating hardness [40]. The physically mixed coatings had few crosslinks. Adding lignin suggested a strong interface between lignin and polymer, which slightly increases the coating hardness [42].

The load-displacement curves during the multi load test of chemically synthesised lignin-PU coatings are shown in Fig. 10. The calculated hardness is shown in Table 3. The hardness was reduced with increasing load, which we assign to the indentation size effect [43,44]. The ratio of the lignin-PU to pure PU hardness is shown in Table S5. The hardness of coating at the same load increased significantly when the lignin content increased. The indentation hardness of the C5 coating increased by one order of magnitude compared with the pure PU coating. And the indentation hardness of C10 and C15 was three orders of magnitude higher than that of the PU coating. The increase in hardness is another evidence for the increase in lignin-induced crosslinking degree.

3.5. Nano scratch for lignin-PU coating

The depth as a function of scratch length for the different coatings are shown in Fig. 11(a). For the very soft pure PU coating, we note oscillations in the depth. Similar results have previously been obtained on the

Table 2
Maximum depth and hardness of the lignin-PU coating.

Coating	Max. Depth (nm)	Hardness (MPa)
PU	5494 ± 241	0.23 ± 0.02
C5	3354 ± 209	0.60 ± 0.08
C10	337 ± 11	60.88 ± 4.43
C15	181 ± 14	177.12 ± 32.97

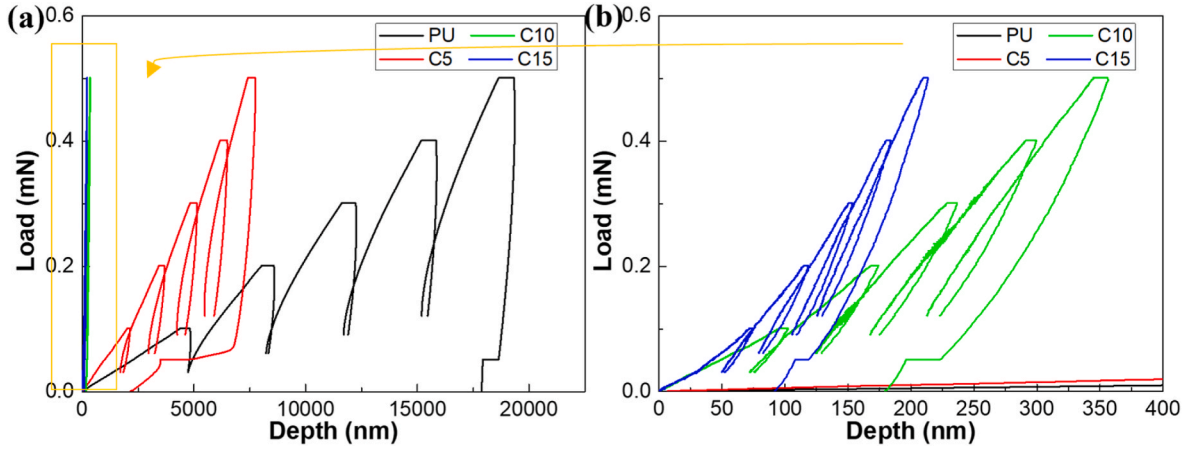

Fig. 10. Load-displacement plots of lignin-PU coating during multi load tests (a) and enlarged parts (b).

Table 3
Hardness of the chemically synthesised lignin-PU coating at different loads during multi load indentation.

Load/ mN	PU Hardness/ MPa	C5 Hardness/ MPa	C10 Hardness/ MPa	C15 Hardness/ MPa
0.1	0.18 ± 0.02	1.04 ± 0.27	293.22 ± 112.87	445.84 ± 121.16
0.2	0.12 ± 0.02	0.70 ± 0.17	270.99 ± 120.08	425.17 ± 106.78
0.3	0.09 ± 0.01	0.56 ± 0.13	244.26 ± 108.31	422.52 ± 91.63
0.4	0.07 ± 0.01	0.48 ± 0.12	210.35 ± 78.43	421.24 ± 76.94
0.5	0.06 ± 0.01	0.43 ± 0.12	183.80 ± 61.24	408.89 ± 69.12

nanoscopic level with AFM for hydrogel samples. It was assigned to pile up in front of the tip, and the oscillations occurred as the tip climbed over the piled-up material [45]. In that study, it was also noted that the pile-up was not due to the fracturing of the material but purely a viscoelastic effect. We interpret our finding similarly.

The maximum depth encountered in each case is reported in Table 4. Clearly, the pure PU coating had the highest scratch depth. C5 coating's scratch depth was around 3850 nm, and C10 and C15 coating had the lowest scratch depth, around 750 and 500 nm, respectively. Physically mixed coatings had similar scratch depth of around 2000 nm.

The friction coefficient (COF) of lignin-PU coatings is reported in Fig. 11(b), and again, the effect of pile-up is noted for the pure PU sample. Clearly, the friction coefficient decreases with the reduce of the hardness of the coating, which suggests that main energy dissipating mechanism for PU is related to the viscoelasticity deformation of the sample rather than sliding in the boundary regime. The COF of PU coating was around 0.9, and the COF of C5 coating was decreased to 0.6. C10 and C15 coatings had the lowest COF, which were both less than 0.2. The low COF of C10 and C15 coatings is consistent with the relatively shallow wear scar found in the friction experiments further characterized by multi scratch tests.

Fig. 12 shows the scratch depth profiles of the chemically synthesised lignin-PU during multi-scratch tests with loads increased from 1 mN to 10 mN, and the zoomed-in graphs for the C10 and C15 coatings are shown in Fig. S6. The maximum scratch depth increased for each scan pass, as shown in Table S6. When the load was 1 mN, the maximum scratch depth of the PU coating increased from around 3800 nm after the first pass to 8200 nm after the eight passes. The maximum scratch depth of the C5 coating gradually increased from around 4500 nm–6500 nm. Compared with all other coatings, the scratch depth of the C10 and C15 coatings were stable at around 300 nm and did not increase significantly

Table 4
Maximum depth of lignin-PU during single scratch measurements.

Coating	Max. Depth/nm
PU	7574 ± 1199
C5	3849 ± 303
C10	747 ± 366
C15	499 ± 174
P5	2483 ± 119
P10	2008 ± 94
P15	1870 ± 100

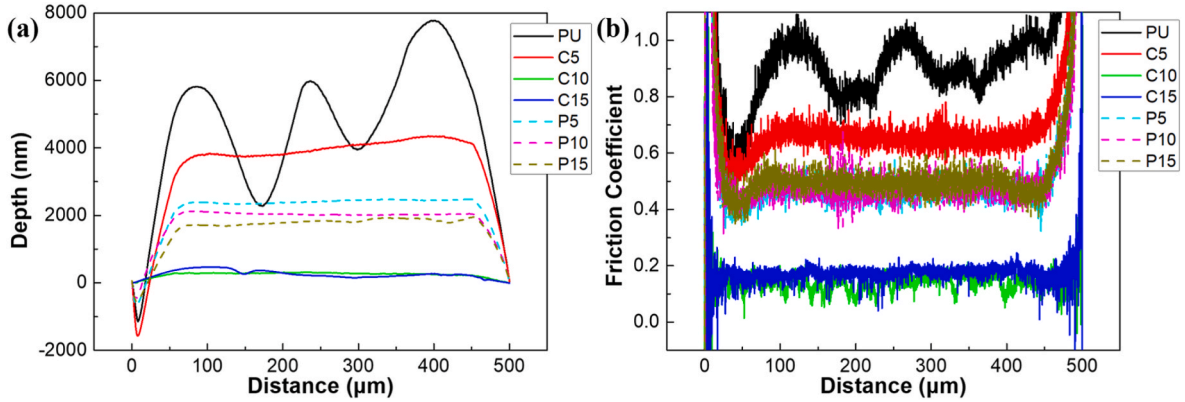

Fig. 11. Depth and friction coefficient of lignin-PU during single scratch measurements.

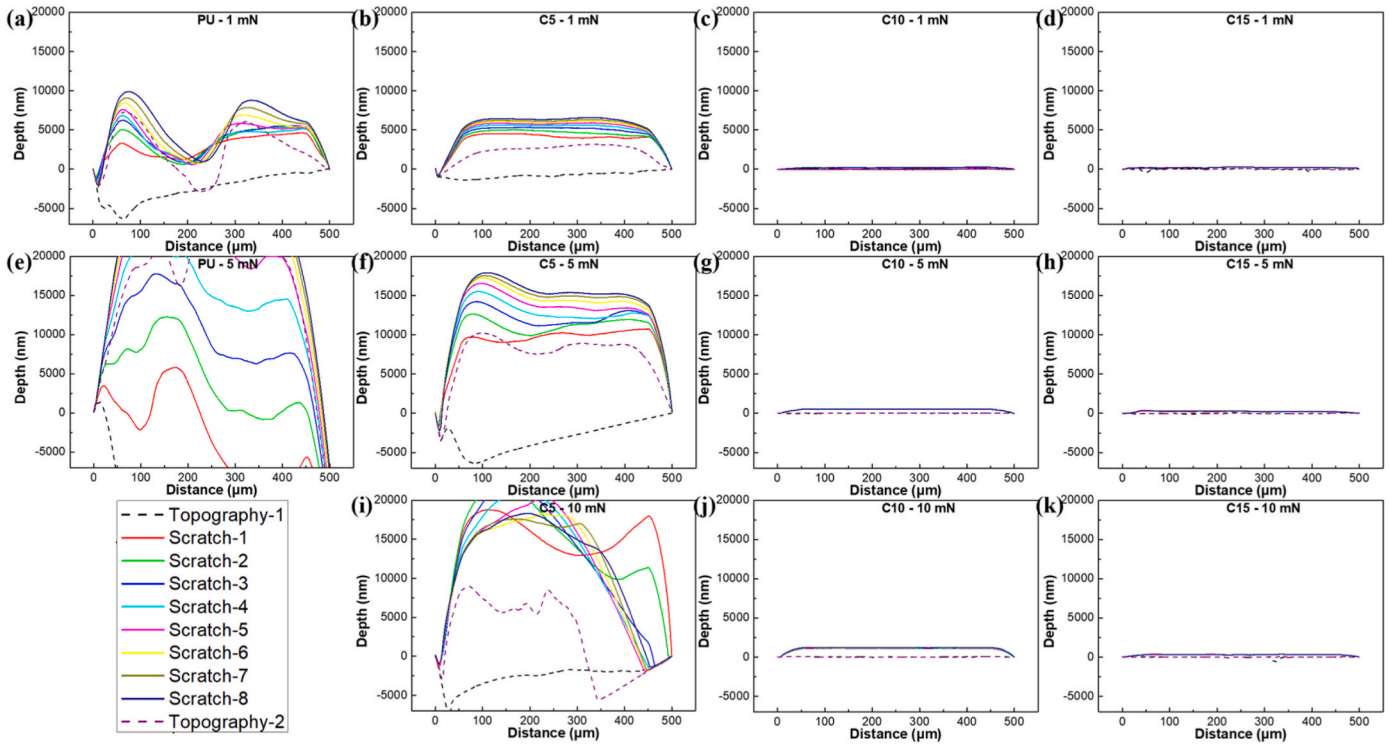

Fig. 12. Depth of chemically synthesised lignin-PU during multi-scratch test with 1 mN load (a-d), 5 mN load (e-h) and 10 mN (i-k).

with the number of paths. When the load increased to 5 mN, the depth of PU coating reached the maximum depth the equipment could measure in the last few scratch passes. The C5 coating's maximum depth increased from 10,800 nm to 17,900 nm. The depth of the C10 coating was around 560 nm, while the depth of the C15 coating was only slightly larger, around 330 nm, compared to that obtained at 1 mN. When the load increased to 10 mN, the depth of the C5 coating also reached the maximum depth of the equipment. The depth of the C10 coating increased to around 1200 nm while the depth of the C15 coating remained at around 340 nm. The scratch depth of the C15 coating

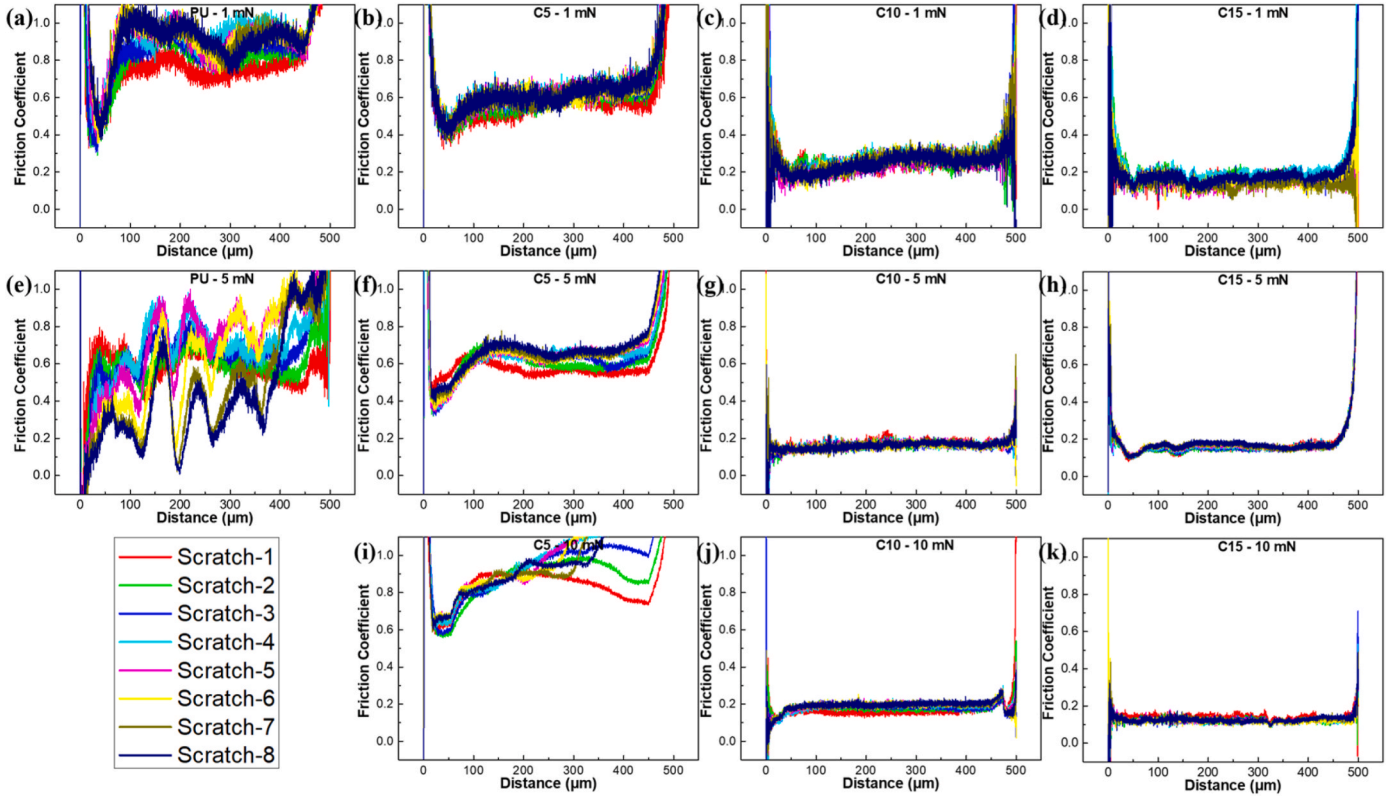

Fig. 13. Friction coefficient of chemically synthesised lignin-PU during nano scratch test with 1 mN load (a-d), 5 mN load (e-h) and 10 mN (i-k).

remained stable during the multi scratch test. This, combined with its shallow depth, indicates that the C15 coating has good wear resistance.

The COF of lignin-PU coatings at different loads obtained during multi scratch measurements are shown in Fig. 13. The trend in the data is consistent with the trend in scratch depth as a lower scratch depth also results in a lower COF. The COF obtained where depths reached the maximum test range of the equipment was not valid and thus not shown. The COF reduced from around 0.8 to 0.15 when lignin content increased from 0 to 15 wt% for chemically synthesised coatings. Notably, for the C10 and C15 coatings the COF remains in the range 0.15–0.20 at all loads explored.

3.6. Wear test for lignin-PU coating

Fig. 14 shows the thickness loss for chemically synthesised lignin-PU coatings under friction tests. The thickness loss decreased with increasing amount of lignin. The PU, C5, C10 and C15 coating had a thickness loss after the complete friction test of 5.1, 3.8, 3.0 and 2.3 μm, respectively. With the addition of lignin, the loss reduction indicates that even a small inclusion of lignin starts to enhance wear resistance, possibly due to lignin acting as a reinforcement or filler, bolstering the material's overall wear resistance. With more lignin, the crosslinking density increased, leading to a denser, wear-resistant matrix. This can explain why coatings with lignin content display better wear resistance. Clearly, the C15 coating had the best wear resistance. Thus, adding lignin up to 15 wt% could improve the wear resistance as well as corrosion protection performance of our lignin-PU coatings.

Considering both EIS data and the wear and friction data reported in this manuscript, it is clear that the C15 coating has the best performance considering both corrosion protection and wear resistance. At lower lignin content, the cross-linking density is too low to provide equally good protection and a higher lignin content leads to too low coating-metal adhesion. It is possible that if the adhesion issue could be resolved, an even higher loading of lignin could perform even better than the C15 coating.

4. Conclusion

An organosolv lignin-based anti-corrosion coating was developed, achieving protection for carbon steel under aggressive corrosion conditions. The optimal coating contained 15 wt% of lignin chemically integrated in a PU matrix. The impedance of the coating with 15 wt% lignin remained at 10^5 Ω•cm^2 after being immersed in 1 M NaCl solution for a week. The developed lignin-PU coating was also evaluated by nanoindentation and nano scratch measurement. The optimized lignin-PU coating had higher hardness, lower maximum scratch depth and lower friction coefficient than coating with less lignin content. These properties make it suitable as both a corrosion protection coating and as an anti-wear coating. As a renewable, green material available in large quantities for coating preparation, lignin-containing coatings may provide a valuable and affordable solution for corrosion and wear protection in the marine environment.

CRediT authorship contribution statement

Di Wang: Conceptualization, Methodology, Validation, Formal analysis, Investigation, Writing - original draft. **Jun Zhao:** Writing - review & editing. **Per Claesson:** Writing - review & editing. **Paul Christakopoulos:** Writing - review & editing. **Ulrika Rova:** Writing - review & editing. **Leonidas Matsakas:** Writing - review & editing. **Erik Ytreberg:** Writing - review & editing. **Lena Granhag:** Writing - review & editing. **Fan Zhang:** Writing - review & editing, Supervision. **Jinshan Pan:** Writing - review & editing, Supervision. **Yijun Shi:** Writing - review & editing, Supervision, Funding acquisition.

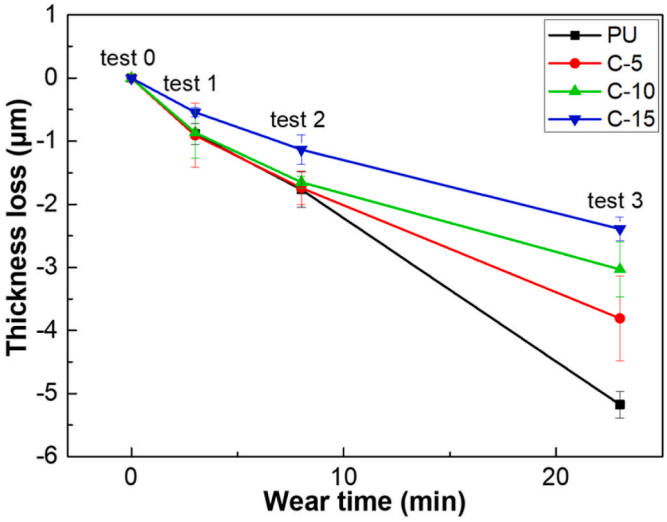

Fig. 14. Wear test results for chemically synthesised lignin-PU coating.

Declaration of competing interest

The authors declare that they have no known competing financial interests or personal relationships that could have appeared to influence the work reported in this paper.

Data availability

Data will be made available on request.

Acknowledgements

The authors thank the Swedish Research Council for Environment, Agricultural Sciences and Spatial Planning (Formas, Project No. 2022-01047, 2021-00728, 2020-01258). Dr. Fan Zhang acknowledges the financial support from the Engineering and Physical Sciences Research Council (EPSRC) under the grant reference EP/Y022009/1.

Appendix A. Supplementary data

Supplementary data to this article can be found online at https://doi.org/10.1016/j.mtchem.2023.101833.

References

[1] E.R. Silva, A.V. Tulcidas, O. Ferreira, R. Bayón, A. Igartua, G. Mendoza, F.J. M. Mergulhão, S.I. Faria, L.C. Gomes, S. Carvalho, J.C.M. Bordado, Assessment of the environmental compatibility and antifouling performance of an innovative biocidal and foul-release multifunctional marine coating, Environ. Res. 198 (2021), 111219, https://doi.org/10.1016/j.envres.2021.111219.

[2] H.S. El-Sheshtawy, M.R. Sofy, D.A. Ghareeb, G.A. Yacout, M.A. Eldemellawy, B. M. Ibrahim, Eco-friendly polyurethane acrylate (PUA)/natural filler-based composite as an antifouling product for marine coating, Appl. Microbiol. Biotechnol. 105 (18) (2021) 7023–7034, https://doi.org/10.1007/s00253-021-11501-w.

[3] C. Xie, H. Guo, W. Zhao, L. Zhang, Environmentally friendly marine antifouling coating based on a synergistic strategy, Langmuir 36 (9) (2020) 2396–2402, https://doi.org/10.1021/acs.langmuir.9b03764.

[4] B. Liu, Z.-g. Fang, H.-b. Wang, T. Wang, Effect of cross linking degree and adhesion force on the anti-corrosion performance of epoxy coatings under simulated deep sea environment, Prog. Org. Coating 76 (12) (2013) 1814–1818, https://doi.org/10.1016/j.porgcoat.2013.05.022.

[5] Z. Mahidashti, T. Shahrabi, B. Ramezanzadeh, The role of post-treatment of an ecofriendly cerium nanostructure Conversion coating by green corrosion inhibitor on the adhesion and corrosion protection properties of the epoxy coating, Prog. Org. Coating 114 (2018) 19–32, https://doi.org/10.1016/j.porgcoat.2017.09.015.

[6] R. Mohammadkhani, M. Ramezanzadeh, S. Akbarzadeh, G. Bahlakeh, B. Ramezanzadeh, Graphene oxide nanoplatforms reduction by green plant-sourced organic compounds for construction of an active anti-corrosion coating;

experimental/electronic-scale DFT-D modeling studies, Chem. Eng. J. 397 (2020), 125433, https://doi.org/10.1016/j.cej.2020.125433.
[7] J.A. Callow, M.E. Callow, Trends in the development of environmentally friendly fouling-resistant marine coatings, Nat. Commun. 2 (1) (2011) 244, https://doi.org/10.1038/ncomms1251.
[8] Y. Li, C. Ning, Latest research progress of marine microbiological corrosion and bio-fouling, and new approaches of marine anti-corrosion and anti-fouling, Bioact. Mater. 4 (2019) 189–195, https://doi.org/10.1016/j.bioactmat.2019.04.003.
[9] M. Izadi, T. Shahrabi, B. Ramezanzadeh, Active corrosion protection performance of an epoxy coating applied on the mild steel modified with an eco-friendly sol-gel film impregnated with green corrosion inhibitor loaded nanocontainers, Appl. Surf. Sci. 440 (2018) 491–505, https://doi.org/10.1016/j.apsusc.2018.01.185.
[10] B. Ramezanzadeh, M.M. Attar, Cathodic delamination and anticorrosion performance of an epoxy coating containing nano/micro-sized ZnO particles on Cr (III)-Co(II)/Cr(III)-Ni(II) posttreated steel samples, Corros 69 (8) (2013) 793–803, https://doi.org/10.5006/0841.
[11] A.W. Momber, T. Marquardt, Protective coatings for offshore wind energy devices (OWEAs): a review, J. Coating Technol. Res. 15 (1) (2018) 13–40, https://doi.org/10.1007/s11998-017-9979-5.
[12] A.W. Momber, P. Plagemann, V. Stenzel, Performance and integrity of protective coating systems for offshore wind power structures after three years under offshore site conditions, Renew. Energy 74 (2015) 606–617, https://doi.org/10.1016/j.renene.2014.08.047.
[13] A. López-Ortega, J.L. Arana, E. Rodríguez, R. Bayón, Corrosion, wear and tribocorrosion performance of a thermally sprayed aluminum coating modified by plasma electrolytic oxidation technique for offshore submerged components protection, Corrosion Sci. 143 (2018) 258–280, https://doi.org/10.1016/j.corsci.2018.08.001.
[14] A. Dastpak, K. Yliniemi, M. de Oliveira Monteiro, S. Höhn, S. Virtanen, M. Lundström, B. Wilson, From waste to valuable resource: lignin as a sustainable anti-corrosion coating, Coat 8 (12) (2018), https://doi.org/10.3390/coatings8120454.
[15] J. Carlos de Haro, L. Magagnin, S. Turri, G. Griffini, Lignin-based anticorrosion coatings for the protection of aluminum surfaces, ACS Sustain. Chem. Eng. 7 (6) (2019) 6213–6222, https://doi.org/10.1021/acssuschemeng.8b06568.
[16] P.J.M. Suhas, M.M.L. Carrott, Ribeiro Carrott, Lignin – from natural adsorbent to activated carbon: a review, Bioresour. Technol. 98 (12) (2007) 2301–2312, https://doi.org/10.1016/j.biortech.2006.08.008.
[17] S. Chatterjee, T. Saito, Lignin-derived advanced carbon materials, ChemSusChem 8 (23) (2015) 3941–3958, https://doi.org/10.1002/cssc.201500692.
[18] J.M. Rosas, R. Berenguer, M.J. Valero-Romero, J. Rodríguez-Mirasol, T. Cordero, Preparation of different carbon materials by thermochemical conversion of lignin, Front. Mater. 1 (2014), https://doi.org/10.3389/fmats.2014.00029.
[19] T. Ju, Z. Zhang, Y. Li, X. Miao, J. Ji, Continuous production of lignin nanoparticles using a microchannel reactor and its application in UV-shielding films, RSC Adv. 9 (43) (2019) 24915–24921, https://doi.org/10.1039/c9ra05064g.
[20] M. Farooq, T. Zou, G. Riviere, M.H. Sipponen, M. Osterberg, Strong, ductile, and waterproof cellulose nanofibril composite films with colloidal lignin particles, Biomacromolecules 20 (2) (2019) 693–704, https://doi.org/10.1021/acs.biomac.8b01364.
[21] E. Rojo, M.S. Peresin, W.W. Sampson, I.C. Hoeger, J. Vartiainen, J. Laine, O. J. Rojas, Comprehensive elucidation of the effect of residual lignin on the physical, barrier, mechanical and surface properties of nanocellulose films, Green Chem. 17 (3) (2015) 1853–1866, https://doi.org/10.1039/c4gc02398f.
[22] V. Ugartondo, M. Mitjans, M.P. Vinardell, Comparative antioxidant and cytotoxic effects of lignins from different sources, Bioresour. Technol. 99 (14) (2008) 6683–6687, https://doi.org/10.1016/j.biortech.2007.11.038.
[23] X. Song, S. Tang, X. Chi, G. Han, L. Bai, S.Q. Shi, Z. Zhu, W. Cheng, Valorization of lignin from biorefinery: colloidal lignin micro-nanospheres as multifunctional bio-based fillers for waterborne wood coating enhancement, ACS Sustain. Chem. Eng. 10 (35) (2022) 11655–11665, https://doi.org/10.1021/acssuschemeng.2c03590.
[24] M. Salzano de Luna, Recent trends in waterborne and bio-based polyurethane coatings for corrosion protection, Adv. Mater. Interfac. (2022), https://doi.org/10.1002/admi.202101775.
[25] Y. Tong, S. Bohm, M. Song, The capability of graphene on improving the electrical conductivity and anti-corrosion properties of Polyurethane coatings, Appl. Surf. Sci. 424 (2017) 72–81, https://doi.org/10.1016/j.apsusc.2017.02.081.
[26] J. Chen, F. Li, Y. Luo, Y. Shi, X. Ma, M. Zhang, D.W. Boukhvalov, Z. Luo, A self-healing elastomer based on an intrinsic non-covalent cross-linking mechanism, J. Mater. Chem. A 7 (25) (2019) 15207–15214, https://doi.org/10.1039/c9ta03775f.
[27] C. Liang, U.R. Gracida-Alvarez, E.T. Gallant, P.A. Gillis, Y.A. Marques, G. P. Abramo, T.R. Hawkins, J.B. Dunn, Material flows of polyurethane in the United States, Environ. Sci. Technol. 55 (20) (2021) 14215–14224, https://doi.org/10.1021/acs.est.1c03654.
[28] Z. Wu, P.P. Thoresen, L. Matsakas, U. Rova, P. Christakopoulos, Y. Shi, Facile synthesis of lignin-Castor oil-based oleogels as green lubricating greases with excellent lubricating and antioxidation properties, ACS Sustain. Chem. Eng. (2023), https://doi.org/10.1021/acssuschemeng.3c01801.
[29] D. Wang, J. Zhao, F. Zhang, P. Claesson, J. Pan, Y. Shi, In-situ coating wear condition monitoring based on solid-liquid triboelectric nanogenerator and its mechanism study, Nano Energy 112 (2023), 108479, https://doi.org/10.1016/j.nanoen.2023.108479.
[30] J. Chen, Z. Luo, R. An, P. Marklund, M. Björling, Y. Shi, Novel intrinsic self-healing poly-silicone-urea with super-low ice adhesion strength, Small 18 (22) (2022), 2200532, https://doi.org/10.1002/smll.202200532.
[31] Z. Wu, J. Chen, D.W. Boukhvalov, Z. Luo, L. Zhu, Y. Shi, A new triboelectric nanogenerator with excellent electric breakdown self-healing performance, Nano Energy 85 (2021), https://doi.org/10.1016/j.nanoen.2021.105990.
[32] L.W. Hill, Calculation of crosslink density in short chain networks, Prog. Org. Coating 31 (3) (1997) 235–243, https://doi.org/10.1016/S0300-9440(97)00081-7.
[33] C.G. Mothé, C.R. de Araújo, Properties of polyurethane elastomers and composites by thermal analysis, Thermochim. Acta 357–358 (2000) 321–325, https://doi.org/10.1016/S0040-6031(00)00403-2.
[34] F.M.B. Coutinho, M.C. Delpech, Degradation profile of films cast from aqueous polyurethane dispersions, Polym. Degrad. Stabil. 70 (1) (2000) 49–57, https://doi.org/10.1016/S0141-3910(00)00087-2.
[35] J. Cheng, N. Mei, S. Chen, P. Bai, B. Shen, J. Pan, F. Zhang, Interactions in composite film formation of mefp-1/graphene on carbon steel, Coat 11 (10) (2021) 1161, https://doi.org/10.3390/coatings11101161.
[36] T.T.X. Hang, T.A. Truc, N.T. Duong, N. Pébère, M.-G. Olivier, Layered double hydroxides as containers of inhibitors in organic coatings for corrosion protection of carbon steel, Prog. Org. Coating 74 (2) (2012) 343–348, https://doi.org/10.1016/j.porgcoat.2011.10.020.
[37] Y. González-García, S. González, R.M. Souto, Electrochemical and structural properties of a polyurethane coating on steel substrates for corrosion protection, Corrosion Sci. 49 (9) (2007) 3514–3526, https://doi.org/10.1016/j.corsci.2007.03.018.
[38] H. Wang, J. Xu, X. Du, Z. Du, X. Cheng, H. Wang, A self-healing polyurethane-based composite coating with high strength and anti-corrosion properties for metal protection, Compos. B Eng. 225 (2021), 109273, https://doi.org/10.1016/j.compositesb.2021.109273.
[39] Y. Liu, S. Li, J. Zhang, J. Liu, Z. Han, L. Ren, Corrosion inhibition of biomimetic super-hydrophobic electrodeposition coatings on copper substrate, Corrosion Sci. 94 (2015) 190–196, https://doi.org/10.1016/j.corsci.2015.02.009.
[40] A. Roy, L. Mu, Y. Shi, Tribological properties of polyimide coating filled with carbon nanotube at elevated temperatures, Polym. Compos. 41 (7) (2020) 2652–2661, https://doi.org/10.1002/pc.25564.
[41] W.C. Oliver, G.M. Pharr, An improved technique for determining hardness and elastic modulus using load and displacement sensing indentation experiments, J. Mater. Res. 7 (6) (1992) 1564–1583, https://doi.org/10.1557/JMR.1992.1564.
[42] K. Waseem, S. Rahul, S. Parveen, Carbon nanotube-based polymer composites: synthesis, properties and applications, in: B. Mohamed Reda, H. Inas Hazzaa (Eds.), Carbon Nanotubes, IntechOpen, Rijeka, 2016, https://doi.org/10.5772/62497. Ch. 1.
[43] H. Li, R.C. Bradt, The indentation load/size effect and the measurement of the hardness of vitreous silica, J. Non-Cryst. Solids 146 (1992) 197–212, https://doi.org/10.1016/S0022-3093(05)80492-2.
[44] F. Alisafaei, C.-S. Han, Indentation depth dependent mechanical behavior in polymers, Adv. Condens. Matter Phys. (2015), 391579, https://doi.org/10.1155/2015/391579, 2015.
[45] G. Li, I. Dobryden, E.J. Salazar-Sandoval, M. Johansson, P.M. Claesson, Load-dependent surface nanomechanical properties of poly-HEMA hydrogels in aqueous medium, Soft Matter 15 (38) (2019) 7704–7714.